Single-molecule measurements of importin α/cargo complex dissociation at the nuclear pore

Changxia Sun, Weidong Yang*, Li-Chun Tu, and Siegfried M. Musser†

Department of Molecular and Cellular Medicine, College of Medicine, Texas A&M Health Science Center, 1114 TAMU, College Station, TX 77843

Edited by Karsten Weis, University of California, Berkeley, CA, and accepted by the Editorial Board April 8, 2008 (received for review November 15, 2007)

Macromolecules are transported between the cytoplasm and the nucleoplasm of eukaryotic cells through nuclear pore complexes (NPCs). Large (more than ≈40 kDa) transport cargoes imported into the nucleus typically form a complex with at least one soluble transport cofactor of the importin (Imp) β superfamily. Many cargoes require an accessory cofactor, Imp α, which binds to Imp β and to the nuclear localization sequence on the cargo. We previously reported the use of narrow-field epifluorescence microscopy to directly monitor cargoes in transit through NPCs in permeabilized cells. We now report an expanded approach in which single-molecule fluorescence resonance energy transfer (FRET) is used to detect the disassembly of Imp α/cargo complexes as they transit through NPCs. We found that CAS, the recycling cofactor for Imp α, and RanGTP are essential for this dissociation process. After Imp α/cargo complex dissociation, most Imp α and cargo molecules entered the nucleoplasm. In contrast, the majority of Imp α/cargo complexes that did not dissociate at the NPC in the presence of CAS and RanGTP returned to the cytoplasm. These data are consistent with a model in which Imp α/cargo complexes are dissociated on the nucleoplasmic side of the NPC, and this dissociation requires both CAS and RanGTP.

FRET | nuclear transport | single-molecule fluorescence

Nuclear pore complexes (NPCs) mediate the bidirectional transport of proteins and RNAs across the double-membrane nuclear envelope (NE) of eukaryotic cells. They are comprised of ≈30 different nuclear pore proteins (Nups), each present in an integer multiple of eight copies (1–3). The pore itself is ≈90 nm long and is ≈50 nm wide at its narrowest point. Flexible filaments extend out from the pore ≈50 nm into the cytoplasm, and a basket structure extends ≈75 nm into the nucleoplasm (1, 4). The pore is filled by natively unfolded (disordered) and highly flexible protein structures containing thousands of phenylalanine-glycine (FG) repeat motifs (3, 5–8). This FG-network provides a selectivity filter, allowing small molecules (less than ≈20–40 kDa) to diffuse through and rejecting most larger molecules. Larger molecules (up to ≈25 MDa) penetrate the FG-network with the assistance of transport receptors of the importin (Imp) β superfamily, which directly interact with the FG repeats (9–11). Import complexes consisting of Imp β, Imp α, and cargo are dissociated after transport by RanGTP, the GTP-bound form of the G protein Ran (12). Imp β is recycled to the cytoplasm in a complex with RanGTP, and Imp α is recycled in a complex with CAS and RanGTP. Activation of the Ran GTPase by the cytoplasmically located RanGAP frees Imp β and Imp α for another round of cargo transport (13–15; for recent reviews, see refs. 9–11).

Numerous mechanisms of Imp α/cargo complex dissociation have been proposed. One possibility is that Imp α/cargo complexes dissociate spontaneously, and an autoinhibitory sequence in the N-terminal Imp β binding domain of Imp α inhibits cargo rebinding (16–18). Spontaneous dissociation could occur in <1 s, assuming a diffusion-limited second-order binding constant ($>10^8$ $M^{-1}{\cdot}s^{-1}$) and a K_D of ≈40 nM (19, 20). Although potentially fast, this mechanism is unlikely to function during transport events that occur on the 1- to 10-ms time scale (21). In a bead binding assay, the mean dissociation time was much longer ($\tau = \approx 9$ min) (16), although this was probably due, at least in part, to a high avidity. According to a second model, binding of a CAS/RanGTP complex to Imp α promotes dissociation of the Imp α/cargo complex (15, 16, 22). In principle, this mechanism could function within the NPC or within the nucleoplasm. According to a third mechanism, NUP50 (Nup2p in yeast), a nuclear pore protein, promotes dissociation of the Imp α/cargo complex (22–27). Because NUP50 is located on the nuclear basket, this model predicts that the Imp α/cargo dissociation event occurs near the end of cargo translocation through the NPC. CAS and RanGTP could also function with NUP50 to promote Imp α/cargo complex dissociation at the NPC.

To distinguish between the above Imp α/cargo complex dissociation mechanisms, we expanded the previously developed single-molecule narrow-field epifluorescence approach (21, 28, 29) to measure FRET between the individual protein components of Imp α/cargo complexes. The major advantage of this approach is the ability to monitor the position and oligomerization state of Imp α and the cargo during real time trafficking of these molecules through intact NPCs. Nucleocytoplasmic transport is inherently a nonequilibrium process, and thus, as we show, these measurements can identify a kinetically stable species that is not readily predicted from equilibrium affinity constants.

Results and Discussion

Simultaneous Detection of Position and Oligomerization State of Imp α1 and Cargo. In earlier work, we used narrow-field epifluorescence microscopy to visualize the transport of individual cargo molecules thorough NPCs in permeabilized HeLa cells (21, 28, 29). Here, we have labeled the four solvent accessible cysteines of human Imp α1 and the model cargo NLS-2xGFP(4C) with Alexa Fluor 568 (donor dye) or Alexa Fluor 647 (acceptor dye). Control experiments indicated that the Imp α1/cargo binding affinity and the NPC interaction time of the cargo were minimally affected by the presence of fluorescent dyes on Imp α1; the cargo interaction frequency was not affected [supporting information (SI) Fig. S1]. The basic assumption of our approach was that if Imp α1 and the cargo were bound together in a complex, the donor and acceptor dyes would be sufficiently close such that FRET would be observed. When they dissociated, the FRET signal would be lost. This assumption is supported by the use of FRET to determine binding affinity (Fig. S1). A typical single-molecule transport event is shown in Fig. 1*A* and Movie S1. The fluorescence signals of the donor and acceptor dyes were

Author contributions: C.S., W.Y., and S.M.M. designed research; C.S. and W.Y. performed research; L.-C.T. contributed new reagents/analytic tools; C.S., W.Y., and S.M.M. analyzed data; and C.S. and S.M.M. wrote the paper.

The authors declare no conflict of interest.

This article is a PNAS Direct Submission. K.W. is a guest editor invited by the Editorial Board.

*Present address: Department of Biological Science, Bowling Green State University, Bowling Green, OH 43403.

†To whom correspondence should be addressed. E-mail: smusser@tamu.edu.

This article contains supporting information online at www.pnas.org/cgi/content/full/0710867105/DCSupplemental.

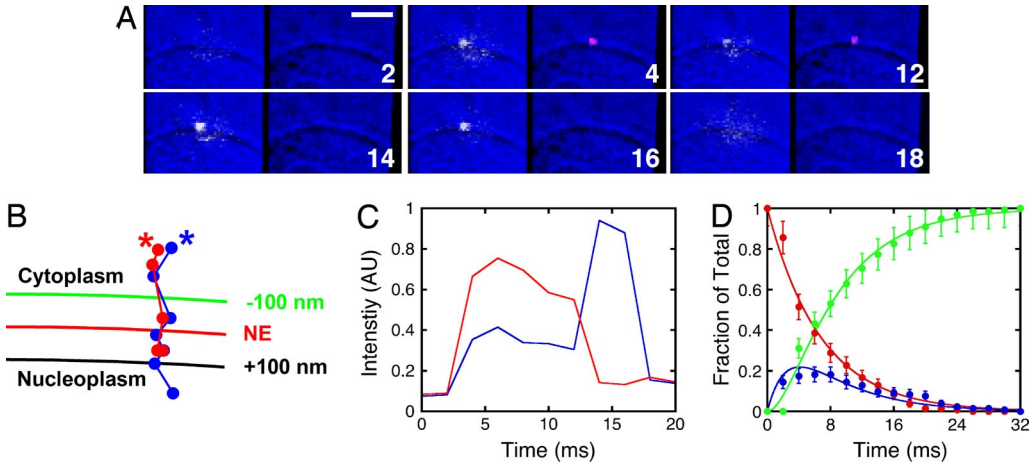

Fig. 1. Interaction between Imp α1 and cargo detected by single molecule FRET during nuclear transport. (*A*) Video frames showing the disappearance of FRET between Alexa Fluor 568–Imp α1 (yellow, *Left*) and Alexa Fluor 647–NLS–2xGFP(4C) (red, *Right*). The bright-field background image (blue) shows the position of the NE as a centrally located curve that bisects the images. Numbers denote time (ms). (Scale bar: 5 μm.) [CAS] = 1.3 μM; [Imp α1] = 0.1 nM; [cargo] = 250 nM; [Imp β1] = 0.5 μM; [Ran] = 2 μM; [NTF2] = 1 μM; [GTP] = 1 mM. (*B* and *C*) Particle trajectories (*B*) and intensity time traces (*C*) for the interaction event in *A*. Asterisks identify the trajectory beginnings. Blue, Imp α1; red, cargo. (*D*) Global fit (Berkeley Madonna) for the decomposition of Imp α1/cargo complexes (A $\rightarrow$ B $\rightarrow$ C) as described in the text (τ_1 = 6.7 $\pm$ 0.3 ms; τ_2 = 2.7 $\pm$ 0.8 ms; n = 132). Red, A; blue, B; green, C.

visualized simultaneously by splitting the fluorescence emission with a dichroic filter onto two opposite halves of the same camera. Upon illumination at 568 nm, the fluorescence emission from the acceptor dyes (on the cargo) was initially observed at the same location as the fluorescence emission from the donor dyes (on Imp α1), consistent with the presence of an Imp α1/cargo complex (Fig. 1*B*). The FRET efficiency was 50 $\pm$ 9% (Fig. S2). The acceptor signal was subsequently lost with a concomitant enhancement of the donor signal (Fig. 1*C*), consistent with the dissociation of cargo from the Imp α1 molecule. The donor signal was lost after the Imp α1 molecule had moved away from the NPC (Fig. 1*B*), consistent with diffusion out of the focal plane. The photobleaching time of the labeled Imp α1 and cargo molecules under these conditions was >140 ms (*Materials and Methods*). Thus, the loss of fluorescence was not due to photobleaching for the vast majority of the observed events.

Kinetics of Imp α1/Cargo Complex Dissociation. By simultaneously detecting FRET and the position of the detectable particles, we determined whether dissociation of Imp α1/cargo complexes occurred at the NPC and where the molecule with the donor dyes went after complex dissociation at the NPC. When an Imp α1 molecule that was originally part of an Imp α1/cargo complex entered the nucleus alone, the following three distinct states were directly identified: (A) the Imp α1/cargo complex bound to the NPC; (B) cargo-free Imp α1 bound to the NPC; and (C) cargo-free Imp α1 that had dissociated from the NPC. By synchronizing the dissociation kinetics for many single-molecule events to the time point at which Imp α1/cargo complexes bound to the NPC, pseudo-first-order rate constants were determined for the A $\rightarrow$ B $\rightarrow$ C process by global-fitting the fraction of each species present as a function of time. At 0.5 μM Imp β and 1.3 μM CAS, τ_1 (A $\rightarrow$ B) was 6.7 $\pm$ 0.3 ms and τ_2 (B $\rightarrow$ C) was 2.7 $\pm$ 0.8 ms (Fig. 1*D*). A similar picture was obtained when the donor and acceptor dye positions were switched, although the cargo appears to exit the NPC first, $\approx$2-fold faster than Imp α1 (Fig. S3).

Influence of CAS on Imp α1/Cargo Complex Dissociation Efficiency at the NPC. Dissociation of Imp α1/cargo complexes depended strongly on the CAS concentration. In the absence of CAS, 0% of Imp α1/cargo complexes dissociated at the NPC, and 55 $\pm$ 4% entered the nucleus, in agreement with the results in ref. 21. In contrast, in the presence of 1.3 μM CAS, $\approx$60% of Imp α1/cargo complexes dissociated at the NPC (Fig. 2*A* and Table S1). The total transport efficiencies of the cargo (52 $\pm$ 2%) and Imp α1 (53 $\pm$ 2%) in the presence of 1.3 μM CAS were identical (within error) to that observed in the absence of CAS. However, an asymmetry developed in the presence of 1.3 μM CAS. The majority of Imp α1/cargo complexes that did not dissociate at the NPC returned to the cytoplasm (82–83%). In contrast, for the majority of Imp α1/cargo complexes that did dissociate at the NPC, the molecule with the donor dyes went into the nucleoplasm (75–81%) (Fig. 2*A* and Table S1). The results were similar when the donor and acceptor dye positions were switched (Fig. 2*A* and Table S1); the minor differences observed may result from the differences in the concentrations necessary to detect single molecules (*Materials and Methods*). Based on the Imp α1/cargo complex dissociation efficiency as a function of the CAS concentration, CAS binds to the NPC with an apparent K_D of 16 $\pm$ 3 nM (Fig. 2*B*). This fairly strong affinity does not exclude the possibility that there may be other lower affinity CAS binding sites within the FG-network. The total transport efficiency of Imp α1 and the cargo were not affected by the CAS concentration (Fig. 2*C*). Using fluorescent CAS, we estimated the NPC interaction time for CAS as 28 $\pm$ 1 ms (Fig. 2*D*). Because the CAS binding experiments were performed in the absence of exogeneous cargo and Imp α1, and the photobleaching time of CAS under these conditions was >140 ms (*Materials and Methods*), CAS does not bind to the NPC and wait for an Imp α1/cargo complex before dissociating.

Influence of RanGTP on Imp α1/Cargo Complex Dissociation Efficiency at the NPC. The dissociation of Imp α1/cargo complexes at the NPC required RanGTP (Table 1). The $\approx$4-fold longer NPC interaction times observed for the cargo in the absence of exogeneous RanGTP are consistent with the hypothesis that RanGTP is required to dissociate Imp β1 from the Imp β1/Imp α1/cargo complex. The residual RanGTP retained in permeabilized cells was likely sufficient to dissociate Imp β1 from the Imp β1/Imp α1/cargo complex (albeit at a lower rate). Rigorous depletion of RanGTP by chemical treatment (28) or preincubation with import complexes (data not shown) leads to longer cargo interaction times. In contrast, the residual RanGTP was

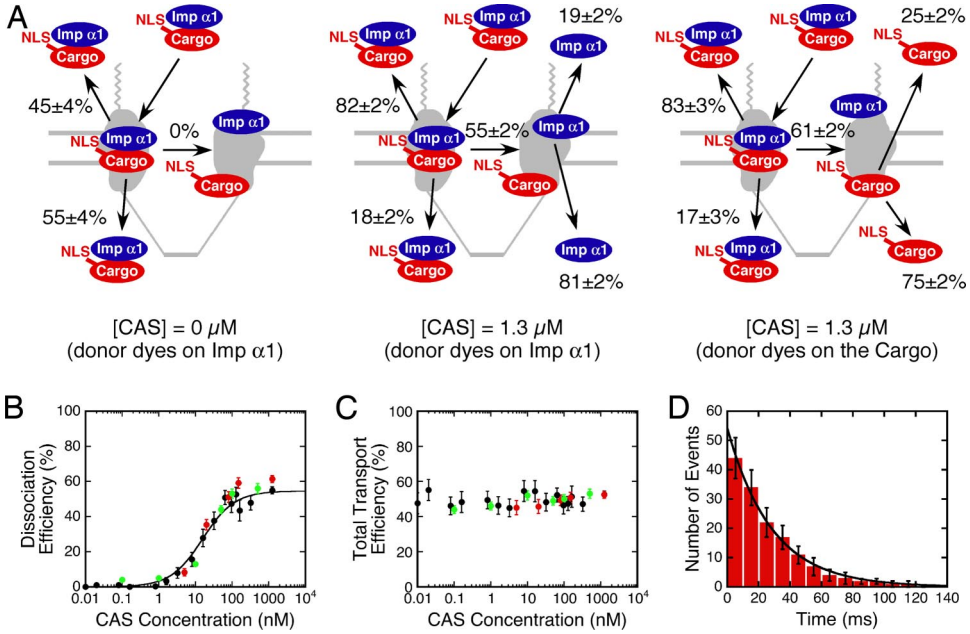

Fig. 2. Effect of CAS concentration on the dissociation efficiency and transport efficiency of Imp α1/cargo complexes. (*A*) Effect of CAS concentration on the oligomerization state and destination of Imp α1 and cargo. Aborted import efficiencies and import efficiencies for Imp α1/cargo complexes that did (*Right*) or did not (*Left*) dissociate are given at the top and bottom of each panel, respectively. Dissociation efficiencies are given in the middle of each panel. (*B* and *C*) The Imp α1/cargo complex dissociation efficiency (apparent $K_D = 16 \pm 3$ nM; fit to black data only) (*B*) and total transport efficiency (*C*) dependence on the CAS concentration. Black, donor dyes on Imp α1, 25% glycerol in buffer; red, donor dyes on the cargo, 25% glycerol in buffer; green, donor dyes on Imp α1, no glycerol in buffer. Fit equation for *B*: $DE = DE_{max} \times [CAS]/(K_D + [CAS])$. (*D*) Histogram of NPC interaction times for CAS ($\tau = 28 \pm 1$ ms; $n = 164$). [Alexa Fluor 647–CAS] = 0.1 nM; [Imp β1] = 0.5 μM; [Ran] = 2 μM; [NTF2] = 1 μM; [GTP] = 1 mM.

insufficient to promote the dissociation of Imp α1/cargo complexes in the presence of CAS (dissociation efficiency $\leq$1%, Table 1). Thus, we conclude that RanGTP is required to promote Imp α1/cargo complex dissociation at the NPC. As expected, the absence of both CAS and RanGTP yielded a low Imp α1/cargo complex dissociation efficiency (0%) and a long cargo interaction time ($\approx$28 ms) (Table S2).

CAS Localization Bias in the NPC Can Explain the Imp α1 and Cargo Exit Bias After Complex Dissociation. Why did most Imp α1/cargo complexes that did not dissociate at the NPC return to the cytoplasm, and why did most of the individual components from dissociated complexes enter the nucleoplasm (Fig. 2*A*)? One explanation is that Imp α1/cargo complexes randomly diffused within the FG-network that occludes the pore and that complexes could only be dissociated at or near the nucleoplasmic exit side of the NPC. According to this picture, complexes that randomly exited on the nucleoplasmic side of the NPC would be preferentially dissociated. We estimated where the dissociation events occurred by determining the last point in each particle trajectory at which FRET was observed. For both entry and abortive transport events, Imp α1/cargo complex dissociation appeared to preferentially occur $\approx$76–87 nm from the NE on the nucleoplasmic side (Figs. 3*A* and *B*). Because CAS was required for Imp α1/cargo complex dissociation at the NPC, one explanation for an asymmetric dissociation profile is that CAS asymmetrically distributes within the NPC. Single molecule localization measurements indicated that CAS spends $\approx$74% of its interaction time with the NPC on the nucleoplasmic side (Fig. 3*C*). This localization bias for CAS can largely explain the $\approx$80% nucleoplasmic exit bias for cargo and Imp α1 after dissociation within the NPC (Fig. 2*A*).

Effect of 25% Glycerol. For most of the experiments reported here, 25% glycerol was added to the transport buffer to reduce the bulk diffusion within the cytoplasmic and nucleoplasmic com-

Table 1. Dissociation of Imp α1/cargo complexes in the presence and absence of exogeneous Ran-GTP

	With 25% glycerol					Without glycerol				
Destination	*n*	Interaction time, ms	Transport efficiency*	Number dissociated	Dissociation efficiency*	*n*	Interaction time, ms	Transport efficiency*	Number dissociated	Dissociation efficiency*
With RanGTP†										
Nucleoplasm	268	7.8 ± 0.3	53 ± 2%	227	55 ± 2%	112	7.6 ± 0.5	51 ± 3%	91	56 ± 3%
Cytoplasm	242	8.0 ± 0.4		53		107	7.8 ± 0.4		32	
Without RanGTP										
Nucleoplasm	126	35 ± 3	48 ± 3%	2	1 ± 2%	97	31 ± 6	45 ± 3%	0	0.5 ± 0.5%
Cytoplasm	138	39 ± 4		1		119	33 ± 5		1	

[Alexa Fluor 568–NLS–2xGFP(4C)] = 0.1 nM; [Alexa Fluor 647–Imp α1] = 250 nM; [CAS] = 1.3 μM; [Imp β1] = 0.5 μM; [NTF2] = 1 μM.
*Transport and dissociation efficiencies were calculated from the data in the nucleoplasm and cytoplasm rows.
†[Ran] = 2 μM; [GTP] = 1 mM.

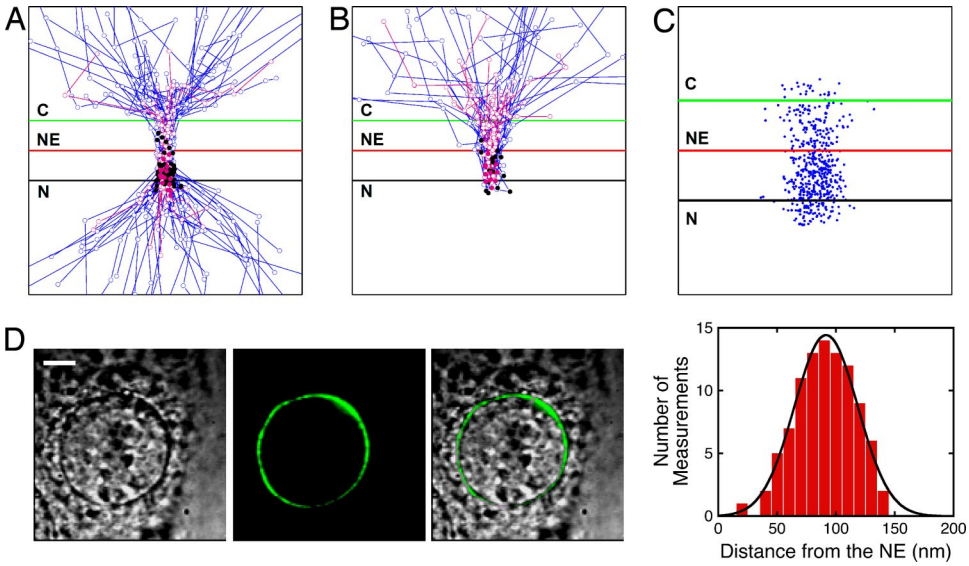

Fig. 3. Location of Imp α1/cargo complex dissociation. (*A* and *B*) Trajectories for Imp α1 that did (n = 50) (*A*) and did not (n = 15) (*B*) enter the nucleus after dissociation from Imp α1/cargo complexes at the NPC. The black dots identify the last location at which FRET was observed (78 ± 30 nm and 77 ± 45 nm from the NE, respectively) in the presence of 25% glycerol (blue trajectories). Control trajectories and the last locations of FRET [87 ± 38 nm (n = 15) and 76 ± 32 nm (n = 10) from the NE, respectively] obtained in the absence of glycerol are shown in pink. For scale, the green and red lines are −100 and +100 nm from the NE. Concentrations are as in Fig. 1*A*, except for the 0% glycerol data where [CAS] = 0.5 μM. C = cytoplasm; N = nucleoplasm. (*C*) Distribution of Alexa Fluor 647–CAS within a 150-nm radius of NPC centers (50 trajectories) under the conditions of Fig. 2*D*. (*D*) Bright-field (*Left*), fluorescence (*Center*), and merged (*Right*) images of a HeLa cell transfected with EGFP2-mNup50. The histogram (Gaussian fit) compares the EGFP2-mNup50 position to the NE, yielding a distance of 92 ± 27 nm from the NE on the nucleoplasmic side (n = 5 cells). No glycerol in buffer. (Scale bar: 5 μm.)

partments. In the presence of 25% glycerol, the originating and destination compartment of the tracked molecule was identified for approximately one-third of the interaction events, as reported in ref. 21. Because glycerol could potentially interfere with NPC function [e.g., like other aliphatic alcohols (30, 31)], some experiments were repeated in the absence of glycerol. The results were the same (within errors) in the presence and absence of glycerol. Specifically, the CAS induced escape asymmetry, the CAS dependence of the dissociation efficiency, and the CAS dependence of the total transport efficiency were similar under both conditions, as shown in Table S1 and Fig. 2 *B* and *C*, respectively. Likewise, the last location at which FRET was observed (Fig. 3 *A* and *B*) and the effect of exogeneous RanGTP on transport efficiency and dissociation efficiency (Table 1) were unchanged under these conditions. Therefore, we conclude that our results are not artifacts of the high glycerol concentration. In the absence of glycerol, the originating and destination compartment of the tracked molecule was identified for approximately one-sixth of the interaction events.

Imp α1 Interaction with NUP50. Numerous groups have postulated that NUP50 (Nup2p) catalyzes Imp α1/cargo complex dissociation when it reaches the nuclear basket region of the NPC (16, 22–27). In control experiments, ≈50% of EGFP2-mNup50 (fusion of 2×EGFP with mouse Nup50) was retained by the NPCs for at least 20 min after permeabilization (Fig. 4*A*). Thus, although EGFP2-mNup50 is rather mobile in live cells (32) and could assist with import as a shuttling cofactor (33), a significant fraction of NUP50 (the wild-type, human, non-GFP-tagged protein) was likely retained for a long period at the NPCs in our permeabilized cells. Therefore, NUP50 alone appears insufficient to promote Imp α1/cargo complex dissociation at the NPC. This result was not predicted from biochemical studies. Although numerous investigators found that NUP50 destabilizes the Imp α/cargo interaction (16, 22, 23, 25, 26), this destabilization seems to be insufficient to cause Imp α/cargo complex dissociation in the context of a functioning NPC on the time scale of transport. The partial loss of NUP50 upon cell permeabilization could explain the incomplete dissociation of Imp α1/cargo complexes that entered the nucleoplasm in the presence of CAS and RanGTP in our experiments (Fig. 2). Based on the fluorescence from EGFP2-mNup50, NUP50 is located 92 ± 27 nm from the NE on the nucleoplasmic side (Fig. 3*D*), consistent with the average dissociation position for the Imp α1/cargo complex (Fig. 3 *A* and *B*). FRET detected between NUP50 and Imp α1 was reduced in the presence of CAS and RanGTP (Fig. 4), consistent with the hypothesis that CAS and RanGTP promote Imp α1 dissociation from NUP50. These data also indicate that the dyes on Imp α1 did not prevent it from interacting with NUP50.

One possibility supported by our data is that CAS, RanGTP, and Imp α/cargo complexes are all simultaneously recruited to NUP50. CAS and RanGTP can be recruited by binding to the FG-repeat domains and Ran-binding domain on NUP50, respectively (34, 35). The FG-repeat domains can potentially serve as an assembly point for CAS/RanGTP complexes. A NUP50/Imp α/cargo complex can be isolated (22, 36), indicating that cargo release is not necessarily immediately induced by the binding of Imp α/cargo complexes to NUP50. Our data support the hypothesis that Imp α/cargo complexes do not dissociate upon binding to NUP50 in the absence of CAS and RanGTP. Although the CAS/RanGTP complex has a weaker affinity for Imp α/cargo complexes than cargo-free Imp α by ≈10-fold, the affinity for Imp α/cargo complexes is still quite high in metazoans (≈10 nM) (15). Thus, as discussed by other investigators, a reasonable scenario is that NUP50 binds both Imp α/cargo and CAS/RanGTP complexes and, by tethering the two complexes together, facilitates dissociation of the cargo from Imp α, ultimately leading to formation of the Imp α/CAS/RanGTP export complex. In other words, NUP50 concentrates various factors in a particular region of the FG-network to coordinate and promote assembly and disassembly reactions through increases in local concentrations (9, 16, 22–27, 37). These various steps may not occur as distinct separable steps, but they may occur in a highly concerted fashion (9).

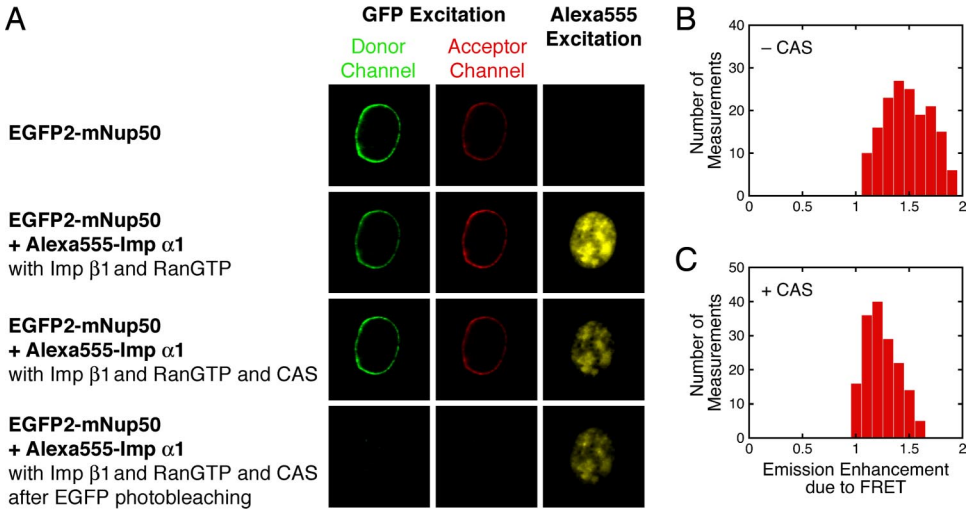

Fig. 4. FRET between EGFP2–mNup50 and Alexa Fluor 555–Imp α1. (*A*) Epifluorescence images of the same cell under the indicated conditions. Approximately 50% of the EGFP2-mNup50 at the NE was retained upon cell permeabilization (top row). The bottom row was obtained after photobleaching the remaining EGFP. Therefore, the fluorescence in the acceptor channel in the top row represents the baseline leakage from the donor channel. The images in the right column, rows 3 and 4, demonstrate that Imp α1 was not photobleached as a consequence of EGFP photobleaching. No glycerol was in the buffer. Proteins were present as indicated: [Alexa Fluor 555–Imp α1] = 0.25 μM; [Imp β1] = 0.5 μM; [Ran] = 2 μM; [GTP] = 1 mM; [NTF2] = 1 μM (present with RanGTP); [CAS] = 1.3 μM. (*B* and *C*) Ratio comparing the acceptor emission signal (center column in *A*) to baseline (top row in *A*) before and after dissociation of Imp α1 from the NPCs in the presence of CAS in *A* (means = 1.5 and 1.2, respectively; n = 8 cells).

Conclusions

We have demonstrated the power of the narrow-field epifluorescence approach by using single-molecule FRET to examine the dissociation of nuclear transport complexes deep within permeabilized cells on the millisecond time scale. We showed that dissociation of Imp α1/cargo complexes occurs at the NPC and that it requires CAS and RanGTP. Further, because most of the cargo and Imp α1 molecules that were observed to enter the nucleoplasm were dissociated at the NPC, this dissociation mechanism dominates. These data strongly argue against a spontaneous dissociation model (16–18) and a model in which NUP50 alone catalyzes the release of cargo from Imp α1 (22, 23). The dissociation events are biased to occur on the nucleoplasmic side of the NPC, minimizing energy waste because RanGTP is preferentially used only for separating Imp α1 and cargo molecules that have a high probability of entering the nucleus. Imp α1/cargo complexes that return to the cytoplasm do not waste a RanGTP molecule in a futile cycle.

The combination of our new data and the NUP50-based model discussed in the last section predicts that Imp α1 enters the nucleoplasm as part of an Imp α1/CAS/RanGTP complex. This is somewhat surprising because such an Imp α1/CAS/RanGTP complex is expected to be a correctly assembled export complex. An alternative is that CAS and RanGTP indirectly mediate Imp α1/cargo complex dissociation and release from the NPC. Previous investigators found that Imp α1 can cycle through NPCs independent of Imp β1 and NLS-cargo (38), suggesting a pathway for cytoplasmic escape of Imp α1 independent of CAS and RanGTP. In either case, it is not understood how the cargo exits from the cytoplasmic side after release from Imp α near the nuclear basket region. Further experiments will be required to examine these issues.

Materials and Methods

Plasmids and Proteins. NLS-2×GFP(4C), Imp β1, Imp α1, Ran, and NTF2 were expressed and purified as in our studies in refs. 21, 28, and 29. CAS was purified as described in refs. 39 and 40, using an expression plasmid obtained from Y.-M. Chook (University of Texas Southwestern, Dallas, TX). The solvent accessible cysteines on NLS-2×GFP(4C), Imp α1, and CAS were reacted with a 20-fold molar excess of maleimide dye (Invitrogen) for 2 h. Labeling ratios of ≈3.5, ≈4, and ≈3.4 dye molecules per protein molecule, respectively, were obtained from single-molecule photobleaching histograms (29). No additional labeling was observed with up to a 160-fold molar excess of dye. The CAS concentration was determined by Coomassie staining an SDS/PAGE gel, using BSA as a standard. Other protein concentrations were determined by the BCA method (Pierce), using BSA as a standard.

EGFP2-mNup50 Cell Line. The EGFP2-mNup50 expression plasmid was obtained from J. Ellenberg (European Molecular Biology Laboratory, Heidelberg, Germany) (32) and used without modification. HeLa cells were transfected with Lipofectamine 2000 according to the manufacturer (Invitrogen). A stable cell line was generated from a single cell after Geneticin (Invitrogen) selection.

Instrumentation. The methodology to monitor the interaction of single molecules with NPCs in permeabilized HeLa cells was established (21, 28, 29). In brief, single-molecule narrow-field epifluorescence measurements (400 μm excitation pinhole) were performed in transport buffer [20 mM Hepes (pH 7.3), 1.5% polyvinylpyrrolidone (360 kDa) 110 mM KOAc, 5 mM NaOAc, 2 mM MgOAc, and 1 mM EDTA], including 25% glycerol unless otherwise indicated by using a Cascade 128+ camera (Roper Scientific) and 2.5 W ArKr mixed-gas ion laser (Spectra Physics). The 400-μm pinhole (placed in the excitation path within a conjugate plane of the specimen plane) improves the signal-to-ratio (S/N) of the epifluorescence approach.

For FRET measurements, the donor and acceptor fluorescence was collected by the same objective lens, passed through a long-pass filter (HQ595LP, Chroma), and split by a dichroic beam splitter (630DCXR; Chroma). The donor and acceptor emission channels were defined by 630 ± 30 nm (HQ630; Chroma) and 692 ± 20 nm (FF01-692; Semrock) band-pass filters, respectively. All filters were mounted in a Dual-View imager (Photometrics). The Metamorph (Universal Imaging) software package was used for data acquisition and processing. All frame integration times were 2 ms. Illumination intensities at the sample plane were ≈1 kW/cm^2 (568 nm and 647 nm). Only the brightest molecules (e.g., those with three or four dye molecules) were analyzed. Photobleaching time is reported as the photobleaching of the first of three (or second of four) dye molecules (≈140 ms). This is a significantly more conservative measure of visualization time than the time required for all dye molecules to photobleach (> 500 ms).

Particle Tracking. The NE position was localized by bright-field imaging (28). The alignment precision between images was determined with 1 μm Tetraspeck microspheres (Invitrogen), and was 4 ± 1 nm (n = 12) between the donor and acceptor fluorescence images, and 15 ± 3 nm (n = 12) between the donor fluorescence and bright-field images. Single molecule trajectories were aligned with the NE and overlaid as described in ref. 21. For FRET, both the donor and

acceptor fluorescence signals were derived from donor excitation (568 nm), resulting in a lower S/N ratio for both donor and acceptor emission intensities than for that observed when only the donor emission was present. During FRET, the localization precision was 46 ± 8 nm and 42 ± 7 nm for Alexa Fluor 568–Imp α1 and Alexa Fluor 647–NLS–2×GFP(4C), respectively, as determined by using coverslip-adsorbed Imp α1/cargo complexes. The average localization difference between donor and acceptor trajectories (e.g., Fig. 1*B*) was ≈12 nm. For immobilized Alexa Fluor 568–Imp α1, the tracking precision was 34 ± 3 nm. In single-molecule transport experiments, the molecule with the donor dyes was present at ≈0.1 nM; the molecule with the acceptor dyes was present at 250 nM. All errors are reported as standard deviations with 68% confidence intervals.

ACKNOWLEDGMENTS. We thank Y. M. Chook for the CAS expression plasmid and J. Ellenberg for the EGFP2-mNup50 expression plasmid. This work was supported by National Institutes of Health Grant GM065534, Department of Defense Grant N00014-02-1-0710, and Welch Foundation Grant BE-1541.

1. Fahrenkrog B, Aebi U (2003) The nuclear pore complex: Nucleocytoplasmic transport and beyond. *Nat Rev Mol Cell Biol* 4:757–766.
2. Rout MP, Aitchison JD (2001) The nuclear pore complex as a transport machine. *J Biol Chem* 276:16593–16596.
3. Cronshaw JM, Krutchinsky AN, Zhang W, Chait BT, Matunis MJ (2002) Proteomic analysis of the mammalian nuclear pore complex. *J Cell Biol* 158:915–927.
4. Stoffler D, *et al.* (2003) Cryo-electron tomography provides novel insights into nuclear pore architecture: Implications for nucleocytoplasmic transport. *J Mol Biol* 328:119–130.
5. Denning DP, Patel SS, Uversky V, Fink AL, Rexach M (2003) Disorder in the nuclear pore complex: The FG repeat regions of nucleoporins are natively unfolded. *Proc Natl Acad Sci USA* 100:2450–2455.
6. Rout MP (2000) The yeast nuclear pore complex: Composition, architecture, and transport mechanism. *J Cell Biol* 148:635–651.
7. Strawn LA, Shen T, Shulga N, Goldfarb DS, Wente SR (2004) Minimal nuclear pore complexes define FG repeat domains essential for transport. *Nat Cell Biol* 6:197–206.
8. Tran EJ, Wente SR (2006) Dynamic nuclear pore complexes: Life on the edge. *Cell* 125:1041–1053.
9. Stewart M (2007) Molecular mechanism of the nuclear import cycle. *Nat Rev Mol Cell Biol* 8:195–208.
10. Cook A, Bono F, Jinek M, Conti E (2007) Structural biology of nucleocytoplasmic transport. *Annu Rev Biochem* 76:647–671.
11. Lim RYH, Aebi U, Fahrenkrog B (2008) Towards reconciling structure and function in the nuclear pore complex. *Histochem Cell Biol* 129:105–116.
12. Görlich D, Panté N, Kutay U, Aebi U, Bischoff FR (1996) Identification of different roles for RanGDP and RanGTP in nuclear protein import. *EMBO J* 15:5584–5594.
13. Bischoff FR, Görlich D (1997) RanBP1 is crucial for the release of RanGTP from importin β-related nuclear transport factors. *FEBS Lett* 419:249–254.
14. Bischoff FR, Klebe C, Kretschmer J, Wittinghofer A, Ponstingl H (1994) RanGAP1 induces GTPase activity of nuclear Ras-related Ran. *Proc Natl Acad Sci USA* 91:2587–2591.
15. Kutay U, Bischoff FR, Kostka S, Kraft R, Gorlich D (1997) Export of importin alpha from the nucleus is mediated by a specific nuclear transport factor. *Cell* 90:1061–1071.
16. Gilchrist D, Mykytka B, Rexach M (2002) Accelerating the rate of disassembly of karyopherin·cargo complexes. *J Biol Chem* 277:18161–18172.
17. Kobe B (1999) Autoinhibition by an internal nuclear localization signal revealed by the crystal structure of mammalian importin α. *Nat Struct Biol* 6:388–397.
18. Harreman MT, *et al.* (2003) Characterization of the auto-inhibitory sequence within the N-terminal domain of importin α. *J Biol Chem* 278:21361–21369.
19. Catimel B, *et al.* (2001) Biophysical characterization of interactions involving importin-alpha during nuclear import. *J Biol Chem* 276:34189–34198.
20. Berg OG, von Hippel PH (1985) Diffusion-controlled macromolecular interactions. *Annu Rev Biophys Biophys Chem* 14:131–160.
21. Yang W, Musser SM (2006) Nuclear import time and transport efficiency depend on importin β concentration. *J Cell Biol* 174:951–961.
22. Gilchrist D, Rexach M (2003) Molecular basis for the rapid dissociation of nuclear localization signals from karyopherin alpha in the nucleoplasm. *J Biol Chem* 278:51937–51949.
23. Matsuura Y, Stewart M (2005) Nup50/Npap60 function in nuclear protein import complex disassembly and importin recycling. *EMBO J* 24:3681–3689.
24. Hood JK, Casolari JM, Silver PA (2000) Nup2p is located on the nuclear side of the nuclear pore complex and coordinates Srp1p/importin-alpha export. *J Cell Sci* 113 (Pt 8):1471–1480.
25. Solsbacher J, Maurer P, Vogel F, Schlenstedt G (2000) Nup2p, a yeast nucleoporin, functions in bidirectional transport of importin alpha. *Mol Cell Biol* 20:8468–8479.
26. Matsuura Y, Lange A, Harreman MT, Corbett AH, Stewart M (2003) Structural basis for Nup2p function in cargo release and karyopherin recycling in nuclear import. *EMBO J* 22:5358–5369.
27. Liu SM, Stewart M (2005) Structural basis for the high-affinity binding of nucleoporin Nup1p to the Saccharomyces cerevisiae importin-β homologue, Kap95p. *J Mol Biol* 349:515–525.
28. Yang W, Gelles J, Musser SM (2004) Imaging of single-molecule translocation through nuclear pore complexes. *Proc Natl Acad Sci USA* 101:12887–12892.
29. Yang W, Musser SM (2006) Visualizing single molecules interacting with nuclear pore complexes by narrow-field epifluorescence microscopy. *Methods* 39:316–328.
30. Ribbeck K, Gorlich D (2002) The permeability barrier of nuclear pore complexes appears to operate via hydrophobic exclusion. *EMBO J* 21:2664–2671.
31. Shulga N, Goldfarb DS (2003) Binding dynamics of structural nucleoporins govern nuclear pore complex permeability and may mediate channel gating. *Mol Cell Biol* 23:534–542.
32. Rabut G, Doye V, Ellenberg J (2004) Mapping the dynamic organization of the nuclear pore complex inside single living cells. *Nat Cell Biol* 6:1114–1121.
33. Lindsay ME, Plafker K, Smith AE, Clurman BE, Macara IG (2002) Npap60/Nup50 is a tri-stable switch that stimulates importin-α:β-mediated nuclear protein import. *Cell* 110:349–360.
34. Loeb JDJ, Davis LI, Fink GR (1993) NUP2, a novel yeast nucleoporin, has functional overlap with other proteins of the nuclear pore complex. *Mol Biol Cell* 4:209–222.
35. Dingwall C, Kandels-Lewis S, Séraphin B (1995) A family of Ran binding proteins that includes nucleoporins. *Proc Natl Acad Sci USA* 92:7525–7529.
36. Booth JW, Belanger KD, Sannella MI, Davis LI (1999) The yeast nucleoporin Nup2p is involved in nuclear export of Importin α/Srp1p. *J Biol Chem* 274:32360–32367.
37. Fahrenkrog B, Koser J, Aebi U (2004) The nuclear pore complex: A jack of all trades? *Trends Biochem Sci* 29:175–182.
38. Miyamoto Y, *et al.* (2002) Importin alpha can migrate into the nucleus in an importin beta- and Ran-independent manner. *EMBO J* 21:5833–5842.
39. Chook YM, Blobel G (1999) Structure of the nuclear transport complex karyopherin-beta2-Ran × GppNHp. *Nature* 399:230–237.
40. Chook YM, Jung A, Rosen MK, Blobel G (2002) Uncoupling Kapbeta2 substrate dissociation and Ran binding. *Biochemistry* 41:6955–6966.